Comparison of climatological planetary boundary layer depth estimates using the GEOS-5 AGCM

Erica L. McGrath-Spangler
Universities Space Research Association
10211 Wincopin Circle, Suite 500 Columbia, MD 21044
and
Global Modeling and Assimilation Office, Code 610.1
NASA Goddard Space Flight Center
8800 Greenbelt Rd.
Greenbelt, MD 20771

Andrea Molod
Earth System Sciences Interdisciplinary Center
University of Maryland
College Park, MD 20740
and
Global Modeling and Assimilation Office, Code 610.1
NASA Goddard Space Flight Center
8800 Greenbelt Rd.
Greenbelt, MD 20771

E. L. McGrath-Spangler	301-614-5838	erica.l.mcgrath-spangler@nasa.gov
A. Molod	301-614-6845	andrea.m.molod@nasa.gov

Abstract

Planetary boundary layer (PBL) processes, including those influencing the PBL depth, control many aspects of weather and climate and accurate models of these processes are important for forecasting changes in the future. However, evaluation of model estimates of PBL depth are difficult because no consensus on PBL depth definition currently exists and various methods for estimating this parameter can give results that differ by hundreds of meters or more. In order to facilitate comparisons between the Goddard Earth Observation System (GEOS-5) and other modeling and observational systems, seven PBL depth estimation methods are used to produce PBL depth climatologies and are evaluated and compared here. All seven methods evaluate the same atmosphere so all differences are related solely to the definition chosen. These methods depend on the scalar diffusivity, bulk and local Richardson numbers, and the diagnosed horizontal turbulent kinetic energy (TKE). Results are aggregated by climate class in order to allow broad generalizations.

The various PBL depth estimations give similar midday results with some exceptions. One method based on horizontal turbulent kinetic energy produces deeper PBL depths in the winter associated with winter storms. In warm, moist conditions, the method based on a bulk Richardson number gives results that are shallower than those given by the methods based on the scalar diffusivity. The impact of turbulence driven by radiative cooling at cloud top is most significant during the evening transition and along several regions across the oceans and methods sensitive to this cooling produce deeper PBL depths where it is most active. Additionally, Richardson number-based methods collapse better at night than methods that depend on the scalar diffusivity. This feature potentially affects tracer transport.

47 1. Introduction

48 The planetary boundary layer (PBL) is crucial to surface-atmosphere exchanges of
49 momentum, energy, moisture, aerosols, carbon, and other chemical tracers. Accurately modeling
50 the PBL character and height in global atmospheric general circulation models (AGCMs) has
51 significant implications for climate and weather predictions, and is made difficult due to the lack
52 of adequate observations. The depth of this layer, in particular, is important for air quality
53 studies since pollutants, aerosols, and carbon dioxide that are emitted near the surface are
54 turbulently mixed throughout the layer and the depth reflects the amount and profile of the
55 turbulence. Inversion studies, which seek to estimate surface fluxes given surface
56 concentrations, are explicitly sensitive to PBL depth errors in atmospheric models [*Gurney et al.*,
57 2002].

58 The PBL parameterization is flawed in many numerical weather models and this leads to
59 prediction errors [*Beljaars*, 1995; *Joffre et al.*, 2001]. These flaws, combined with only limited
60 measurements, contribute to the difficulty of producing a PBL depth comprehensive climatology,
61 despite its importance [*Joffre et al.*, 2001]. In addition, multiple PBL depth definitions exist and
62 these can give different results [*Seidel et al.*, 2010], complicating PBL depth estimation and
63 comparisons between models and observations.

64 Several studies have attempted to understand the uncertainty associated with the use of
65 different PBL depth definitions and found the result to depend substantially on the method
66 chosen. *Vogelezang and Holtslag* [1996] examined the PBL depth by defining it using both bulk
67 and gradient Richardson numbers and found that the choice of Richardson number, the critical
68 number chosen, and the inclusion of surface friction impacted the results. *White et al.* [1999]
69 used summertime data near Nashville, Tennessee to compare the PBL depth estimated by wind

profilers and an airborne differential absorption lidar (DIAL). They found that the different datasets produced similar PBL depths under clear conditions (correlation coefficient of 0.94 and mean offset of 37 m), but the agreement degraded under cloudy conditions (correlation coefficient of 0.87) with a mean difference of about 150 meters.

Seibert et al. [2000] found that all PBL height definition schemes had deficiencies under certain conditions. They examined 7 different datasets and 10 equations commonly used to determine the PBL depth and concluded that the definitions have to be seen in the context of the data used. Likewise, *Seidel et al.* [2010] tested 7 different PBL depth definition methods on radiosonde profiles. Using a single dataset, the estimated PBL depth was found to generally differ by several hundred meters, depending on the method used. The use of different methods in their study produced differences of more than 1 km and even produced different seasonal variations. These differences were statistically significant in practically all comparisons between methods, introducing a structural uncertainty of 10-100% of climatological means. *Seidel et al.* [2010] concluded that it is necessary to compare different PBL depth estimates using the same method. They suggested the development of multiple climatologies using different definitions and the use of the appropriate one for the application desired.

In the present study, seven different methods to compute the PBL depth, based on vertical profiles of the scalar diffusivity, the bulk and local Richardson (Ri) numbers, and the horizontal component of the turbulent kinetic energy (TKE), are incorporated into the Goddard Earth Observation System (GEOS-5) AGCM [*Rienecker et al.*, 2008; *Molod et al.*, 2012] and compared using a single climate simulation. In order to provide insight into implications on the regional and global climate scale, results are aggregated using Köppen-Geiger climate classes [*Peel et al.*, 2007].

93 The purpose of this study is two-fold. First, it analyzes differences among the PBL depth
94 definitions within the GEOS-5 model using the same atmosphere. Second, it enables a
95 comparison among GEOS-5, observations, and other numerical simulations using the same
96 definition so as to evaluate the atmospheric profiles rather than the method used.

97 The following section provides a model description and a description of the PBL depth
98 diagnostics used. The third section presents results, and the final section contains the
99 conclusions.

100 ## 2. Model and PBL Diagnostics

101 ### 2.1 GEOS-5 Model Description

102 The GEOS-5 AGCM is part of the GEOS-5 data assimilation system, an earlier version
103 of which was used for the Modern-Era Retrospective Analysis for Research and Applications
104 (MERRA) [*Rienecker et al.*, 2011]. The latitude-longitude hydrodynamical core of GEOS-5
105 uses the finite volume dynamical core of *Lin* [2004] and the cubed sphere version is based on
106 *Putman and Lin* [2007]. GEOS-5 includes moist physics with prognostic clouds [*Bacmeister et*
107 *al.*, 2006]. The convective scheme is a modified version of the Relaxed Arakawa-Schubert of
108 *Moorthi and Suarez* [1992], the shortwave radiation scheme is that of *Chou and Suarez* [1999],
109 and *Chou et al.* [2001] describe the longwave radiation scheme. The Catchment Land Surface
110 Model is used to determine fluxes at the land/atmosphere interface [*Koster et al.*, 2000] and the
111 surface layer is determined as in *Helfand and Schubert* [1995]. The model uses 72 vertical
112 pressure layers that transition from terrain following near the surface to pure pressure levels
113 above 180 hPa [*Rienecker et al.*, 2008; *Molod et al.*, 2012] and this study uses approximately ½
114 degree horizontal resolution on the cubed sphere. The simulation covers January 1990 through
115 May 2013.

GEOS-5 includes two atmospheric boundary layer turbulent mixing schemes [*Rienecker et al.*, 2008]. The scheme of *Louis et al.* [1982] is used in conjunction with the scheme of *Lock et al.* [2000]. The Lock scheme is a non-local first order scheme in which the diffusivities are computed based on the buoyancy associated with the surface based (positive buoyancy) and the cloud-based radiative cooling (negative buoyancy) "plumes". This scheme has been extended in GEOS-5 so that the unstable surface plume calculation includes moist heating and entrainment [*Rienecker et al.*, 2008]. The Louis scheme is a first order local scheme in which the turbulence diffusivities are computed as functions of the gradient Richardson number. The turbulent length scale is assumed to be related to the PBL height as diagnosed from the Louis-Lock combined eddy diffusivities. The eddy diffusivities used for the AGCM turbulent diffusion are the larger of the Lock or Louis diffusivities at any time step [*Molod et al.*, 2012].

2.2 PBL Depth Diagnostics

Seven different methods for determining the PBL depth are evaluated using the GEOS-5 model based on several different output variables (Table 1). All methods evaluate the same atmospheric profiles and all differences are related solely to the choice of definition. The PBL depth based on the total scalar diffusivity using method 1, is used to compute the turbulent length scale [*Blackadar*, 1962] for the Louis scheme. This PBL depth is termed "active" since it feeds back to the turbulence scheme and determines the vertical extent of mixing. This first method estimates the PBL depth as the model level above which the scalar diffusivity falls below a threshold value of 2 $m^2 s^{-1}$.

The use of the scalar diffusivity to define the PBL depth is further investigated by using a threshold of 10% of the column maximum and linearly interpolating between levels to determine the PBL depth. Method 2 uses the total scalar diffusivity and method 3 uses the surface

buoyancy driven scalar diffusivity, but neglects the radiatively driven component defined by the *Lock et al.* [2000] scheme.

The PBL depth definition used by *Seidel et al.* [2012] and based on the work by *Vogelezang and Holtslag* [1996] is used as the fourth method. *Seidel et al.* [2012] selected this method because of its applicability to radiosondes and model simulations and its suitability for convective and stable boundary layers. This method uses a bulk Richardson number given by:

$$Ri_b(z) = \frac{(\frac{g}{\theta_{vz}})(\theta_{vz}-\theta_{vs})(z-z_s)}{u_z^2+v_z^2}$$

Ri_b is the Richardson number, g is gravity, θ_v is the virtual potential temperature, u and v are the horizontal wind components, and z is height. The subscript s denotes the surface and the surface winds are assumed zero. The Richardson number is evaluated between the surface and successively higher heights, identifying the PBL top as the level at which Ri exceeds a critical value of 0.25. The PBL height is found by linearly interpolating between model levels. Additionally, two other methods use a different version of the Richardson number evaluated between two consecutive levels rather than between the surface and the current height. These methods use a local Richardson number calculated as:

$$Ri(z) = \frac{(\frac{g}{\theta_v})(\theta_{vz1}-\theta_{vz2})(z1-z2)}{(u_{z1}-u_{z2})^2+(v_{z1}-v_{z2})^2}$$

Here, *z2* represents the level height below the height z1 and θ_v without a subscript is the average virtual potential temperature between heights *z1* and *z2*. The fifth method tests a critical Richardson number value of 0 and the sixth tests a critical value of 0.2.

Finally, since the PBL is generally considered turbulent with only sporadic clear air turbulence aloft [*Stull*, 1988], the TKE due to shear is used to estimate the PBL depth in the seventh method. The horizontal TKE is estimated from the wind shear and momentum

161 diffusivity and then the top of the PBL is taken to be the height at which the value falls below a
162 threshold value of 10% of the column maximum.

163 2.3 Climate Classes

164 *Peel et al.* [2007] recently updated the Köppen-Geiger climate classification, taking
165 advantage of advances in data availability and computing power. They did this by using monthly
166 mean precipitation and temperature data from over 4000 stations (plus additional data from
167 stations reporting only temperature or only precipitation) and interpolating between them using a
168 two-dimensional thin-plate spline with tension. The final map is generated on a 0.1°x0.1° grid.
169 The highest station density is in the USA, southern Canada, northeast Brazil, Europe, India,
170 Japan, and eastern Australia while the lowest station data is located in desert, polar, and some
171 tropical regions.

172 *Peel et al.* [2007] used the same classes as the original classification system, but with an
173 updated boundary condition between the temperate and cold climate classes. The classification
174 consists of five main classes consisting of tropical (A), arid (B), temperate (C), cold (D), and
175 polar (E) with further divisions based on seasonal variations in temperature and precipitation.
176 *Peel et al.* [2007] provides a full description of the climate classifications including details on
177 how the classification was determined. The broad climate types are relatively insensitive to
178 temperature trends, including those from global climate change [*Triantafyllou and Tsonis*, 1994;
179 *Peel et al.*, 2007] and are intended to represent long term mean climate conditions and not year-
180 to-year variability.

181 In an effort to generalize the results of this analysis, the computed PBL depths are
182 aggregated by season onto the Köppen-Geiger climate classes, which are regridded to the 1/2°
183 horizontal grid used by GEOS-5 (Figure 1). The Köppen-Geiger climate classes have been used

184 to group rivers worldwide for comparisons of runoff characteristics [*McMahon et al.*, 1992; *Peel*
185 *et al.*, 2004]. Similarly, *Molod and Salmun* [2002] successfully used this technique in their study
186 investigating the implications of using different land surface modeling approaches. Their study
187 aggregated results such as canopy temperature, soil moisture, and turbulent fluxes and they were
188 able to use these results to make generalizations that extend to broad climate regions relevant for
189 global models. These climate classes are a way to characterize similar remote regions and apply
190 findings globally. However, it is important to keep in mind that this classification does not take
191 into account other aspects of the climate system relevant to boundary layer processes.
192 Differences such as intensity of precipitation, elevation, and overlying subsidence are not
193 considered.

194 3. Results

195 3.1 Regimes within Climate Classes

196 The Köppen-Geiger climate classes organize remote land regions together based on
197 temperature and precipitation. However, these regions can have very different large-scale
198 dynamics that also influence the PBL depth such as subsidence, intensity and frequency of
199 precipitation, and terrain. Two examples of this type of variability within climate classes are
200 presented here. The first example is illustrated in Figure 2, which shows the climatological
201 relationship between PBL depth and sensible heat flux for climate class BWh (arid, hot desert) in
202 winter. Each point on the scatter plot represents the seasonal mean midday PBL depth and
203 sensible heat flux for a GEOS-5 grid cell within the BWh climate class.

204 Several different regimes are present associated with different climatic conditions. The
205 Australian deserts (the non-black points, colored according to evaporative fraction), in particular,
206 have two different regimes associated with them during the winter. The first regime at low

sensible heat flux (<100 W m^{-2}) is associated with evaporative fractions above 0.3 while the other regime, characterized by sensible heat fluxes between 100 and 260 W m^{-2} and shallower PBL depths, has evaporative fractions around 0.2. This second regime has less variation of PBL depths with sensible heat, and has a median depth about 260 meters shallower than the first regime. This shows that similar climate and physical proximity cannot explain all PBL depth variability.

The second example is illustrated in Figure 3, which shows the relationship between PBL depth and 10-meter temperature for the tropical rainforest climate class (Af) colored according to relative humidity. In this climate class and the other tropical climate classes, there is a shift in the relationship occurring around 302 K. This temperature is near the wilting point for broadleaf evergreen, the dominant vegetation type in the tropics. At temperatures above the wilting point, the vegetation experiences stress thus severely limiting transpiration and near surface humidity. In these drier conditions, less energy goes in to evaporating water and, by energy balance, more goes in to sensible heat flux. Since sensible heat is much more efficient at growing the PBL than latent heat, the PBL depth increases rapidly with temperature in this drier regime [*Avissar and Pielke*, 1989]. In the regime below the wilting point, transpiration increases with temperature and proceeds with little resistance, wetting the lower atmosphere. In this wetter regime, PBL depth decreases with temperature.

These different regimes and sensitivities of PBL depth to different variables must be kept in mind when examining climatological boundary layer depth. Although the Köppen-Geiger climate classes are able to capture a lot of the variability and are useful for organizing land regions in order to make generalizations and simplify the analysis, they do not capture all the large-scale climate conditions relevant to boundary layer processes. There will therefore be

geographical differences between regions within a climate class that will not be captured by this analysis.

3.2 General Method Behavior

Generally, the PBL depth definitions produce similar results. Differences are highlighted below. Figure 4 shows the seasonal mean diurnal cycle for the cold climate class with dry, hot summer (Dsa during summer 4a and winter 4c) and hot, arid desert (BWh during summer 4b and winter 4d). For these climate classes, the scalar diffusivity methods using a 10% threshold (methods 2 and 3) are insensitive to the use of the radiative plume from the Lock turbulence scheme. The PBL depths estimated using the bulk Richardson number (method 4), the TKE (method 7), and the three scalar diffusivity methods (methods 1, 2, and 3) give comparable midday results over land, giving us confidence in the estimated depth under these conditions.

Although the horizontal TKE definition gives similar midday results to the scalar diffusivity and bulk Richardson number methods under most conditions, during the winter in temperate and cold climates, the horizontal TKE method often gives PBL depths that are 100 meters or more deeper than the other methods (Figure 4c and 4d). This is due to the winter storm tracks and associated increase in wind shear. The horizontal TKE is diagnosed in the model by multiplying the momentum diffusivity by the local wind shear making the horizontal TKE method more sensitive to the wind profile and seasonal changes to it than the other methods. The stronger and deeper wind shear thus produces a deeper turbulent layer and therefore a deeper diagnosed PBL depth based on this variable.

The results from the horizontal TKE method, while consistent with other PBL methods over land, are inconsistent with the other methods over the oceans. The horizontal TKE derived PBL depth gives results as much as 400 meters deeper than the other definitions and have diurnal

253 variability considerably larger. It is therefore suggested that this method not be used to estimate
254 marine boundary layer depths.

255 The methods based on the local Richardson number estimate PBL depths that are several
256 hundred meters shallower at midday than PBL depths using the other methods. This method
257 does not depend greatly on the critical Richardson number chosen as the differences between
258 PBL depths estimated using a critical value of zero are only slightly shallower than PBL depths
259 estimated using a critical value of 0.2. *Seidel et al.* [2012] similarly found small uncertainty
260 associated with the choice of critical value in their study.

261 The Richardson number based methods (local and bulk) collapse better at night than the
262 definitions based on the scalar diffusivity or TKE. This has implications for estimating the
263 shallow nocturnal boundary layer and studies involving tracer transport. For instance, over
264 climate class BWh (arid, hot desert representing such areas as the Sahara and Australian deserts,
265 Figure 4b), the bulk Richardson number nocturnal PBL is well under 500 meters and the local
266 Richardson number PBL depths are only a few hundred meters while the scalar diffusivity
267 methods estimate a PBL depth between 1000 and 1500 meters at night during the summer.

268 3.3 Bulk Richardson vs. Scalar Diffusivity Methods

269 While the bulk Richardson number and scalar diffusivity methods generally give similar
270 midday results, under warm, wet conditions, the estimated daily maximum PBL depth found
271 using the bulk Richardson number method tends to be shallower than the scalar diffusivity
272 methods. This occurs for the tropical rainforest climate class (Figure 5) as well as the other
273 tropical climate classes during their rainy seasons and even for temperate climate classes when it
274 is both warm and there is a lot of precipitation. This difference means that the Richardson
275 number exceeds its critical value at a level below which the scalar diffusivity decreases to its

threshold value. This implies a virtual potential temperature inversion occurring within the layer of relatively high scalar diffusivity. Figure 6 shows the June, July, and August (JJA) seasonal mean vertical profiles of total scalar diffusivity, the scalar diffusivity from the Louis parameterization, and the Richardson number from a typical location within the Amazonian rainforest. The horizontal dashed lines indicate the PBL depth found using the total scalar diffusivity (method 1, Figure 6a) and Richardson number (method 4, Figure 6b). These profiles show that the Richardson number becomes stable below where the scalar diffusivity declines.

This could occur under several different meteorological conditions. There could be a turbulent layer aloft that is not fully decoupled from the surface layer that is being detected by the scalar diffusivity methods, but not the bulk Richardson number method. If the scalar diffusivity predicted by the Louis scheme (Figure 6a) is shallow with its maximum low to the ground, it can be expected that the PBL depth found using the bulk Richardson number might also be shallow. The Louis turbulence parameterization is dependent upon a local Richardson number and so contains some information about the vertical profile of temperature and shear. While this is a different form of the Richardson number from what is used in the bulk Richardson number method, the Louis scheme can provide information about what to expect from the bulk Richardson number method. If, however, the Lock scheme is strongly active aloft due to entrainment or radiation, the scalar diffusivity methods may detect a deeper PBL.

3.4 Impact of radiative plume

The Lock turbulence scheme extends the nonlocal eddy-viscosity based scheme based on *Holtslag and Boville* [1993] to include the effects of radiative cooling at cloud top by positing a turbulent "radiative plume" descending from cloud base due to negative buoyancy associated with radiative cooling. In order to test the impact of the associated radiative plume, the scalar

299 diffusivity method using a threshold of 10% of the column maximum was tested both with
300 (method 2) and without (method 3) the scalar diffusivity associated with the radiative plume.
301 Figure 7 shows the diurnal cycle of the PBL depth difference between the two methods for JJA.
302 At all locations, the PBL depth estimated using the radiative plume was deeper or the same
303 height as that without the plume. The largest differences occurred over land in the summer
304 hemisphere and in the tropics during the evening transition. This result holds for December,
305 January, and February (DJF) as well (not shown). The evening timing is because the radiative
306 plume is sensitive to cloud top. At night, the scalar diffusivities decrease due to the lack of
307 incoming solar radiation, but the diffusivity associated with the radiative plume decreases less
308 proportionally to the other diffusivities since the cloud does not dissipate during the evening
309 transition. The radiative plume scalar diffusivity thus becomes proportionally more important at
310 night and the PBL depth remains deeper. The non-radiative method therefore collapses better at
311 night.

312 In addition to the maxima over land, there are persistent regions of relatively large
313 radiative plume impact over the oceans around 30°N and 45°S. This is due to the way GEOS-5
314 estimates the effective liquid cloud particle radius. GEOS-5 uses an empirical model based on
315 temperature, pressure, and wind speed to estimate this radius. The large differences over oceans
316 are located in regions with a temperature transition, creating a collocation of relatively small
317 prescribed effective radii and boundary layer clouds. In cloudy regions, more shortwave
318 radiation is absorbed in areas with many small droplets than in areas with fewer large droplets.
319 This produces an increase in temperature leading to an enhanced longwave flux, which drives the
320 radiative plume. Since the radiative plume is more active in these locations, PBL methods
321 sensitive to its impact are deeper than if the radiative plume was neglected.

4. Conclusions

Although the PBL depth is important for AGCMs and has implications for climate and weather prediction, observations are limited and no consensus on definition exists. Complicating things further, under certain conditions, different definitions can give significantly different results. This study examines this issue by using seven different methods to define the PBL depth using the same atmosphere so that all differences can be attributed directly to the definition. It is, however, important to point out that this is not an extensive validation. Results are aggregated to Köppen-Geiger climate classes in order to make broad generalizations and simplify the analysis on a global scale. Within these climate classes, different regimes are present that are related to differences in temperature and evaporative fraction. These differences are not captured when the results are aggregated, but the general behavior is represented.

Under most conditions, the bulk Richardson number, scalar diffusivity, and horizontal TKE methods give similar midday results over land. The horizontal TKE definition is more sensitive to winter storms and their associated shear and so estimate deeper midday PBL depths during the winter season. The local Richardson number methods are relatively insensitive to the critical Richardson number used and estimate PBL depths several hundred meters shallower than the other methods. Both the local and bulk Richardson number methods collapse better at night than the scalar diffusivity and TKE methods. For instance, over hot, arid deserts, the bulk Richardson number method estimates a nocturnal PBL depth that is up to a kilometer shallower than the default scalar diffusivity method using a threshold of 2 $m^2 s^{-1}$.

Under warm, moist conditions, the bulk Richardson number method estimates PBL depths that are shallower than those estimated by the scalar diffusivity methods. This indicates that the Richardson number is exceeding its threshold value below the level at which the scalar

345 diffusivity decreases to its threshold value. This response is associated with a maximum in the
346 Louis scheme scalar diffusivity near the surface and Lock scheme scalar diffusivities with
347 maxima higher in the atmosphere.

348 The Lock scheme includes the effects of a radiative plume associated with longwave
349 cloud base cooling. The impact of this effect on PBL depth was found to have its strongest
350 effect over land during the evening transition because of the persistence of cloud cover through
351 the diurnal cycle. Additionally, regions of influence were found in the marine boundary layer
352 related to the way the effective liquid cloud radius is defined in GEOS-5.

353 This study analyzes the sensitivity of the PBL depth in GEOS-5 to the definition chosen
354 under different meteorological conditions. Although each definition was evaluated using
355 identical atmospheres, under various environments the resulting PBL depth could differ by a
356 kilometer or more. This reinforces the recommendation by *Seidel et al.* [2010] that PBL depths
357 be compared only using the same definition. This work also provides multiple climatologies that
358 can be used for evaluation and comparisons in the future with other models and observations
359 using similar definitions. Since the PBL depth in GEOS-5 is not purely diagnostic, but feeds
360 back on the turbulence through the turbulent length scale, the choice of definition is important
361 for vertical mixing and tracer transport. This aspect of the model will be evaluated in future
362 work.

363 Acknowledgments

364 Computing was supported by the NASA Center for Climate Simulation. The research was
365 supported by National Aeronautics and Space Administration grant NNG11HP16A.

366 References

Avissar, R. and R. A. Pielke (1989), A parameterization of heterogeneous land surfaces for atmospheric numerical models and its impact on regional meteorology, Mon. Weather Rev., 117, 2113-2136, doi: http://dx.doi.org/10.1175/1520-0493(1989)117<2113:APOHLS>2.0.CO;2

Bacmeister, J. T., M. J. Suarez, and F. R. Robertson (2006), Rain Reevaporation, Boundary Layer-Convection Interactions, and Pacific Rainfall Patterns in an AGCM, J. Atmos. Sci., 63(12), 3383-3403, doi:10.1175/jas3791.1.

Beljaars, A. C. M. (1995), The impact of some aspects of the boundary layer scheme in the ECMWF model, paper presented at ECMWF Seminar on Parameterization of Subgrid-Scale Physical Processes, ECMWF, Reading, England.

Blackadar, A. K. (1962), The vertical distribution of wind and turbulent exchange in a neutral atmosphere, J. Geophys. Res., 67(8), 3095-3102, doi:10.1029/JZ067i008p03095.

Chou, M.-D., and M. J. Suarez (1999), A solar radiation parameterization for atmospheric studies, 40 pp., in Technical Report Series on Global Modeling and Data Assimilation, edited by M. J. Suarez, NASA, Greenbelt, MD. (http://gmao.gsfc.nasa.gov/pubs/docs/Chou136.pdf)

Chou, M.-D., M. J. Suarez, X.-Z. Liang, and M. M.-H. Yan (2001), A thermal infrared radiation parameterization for atmospheric studies, 56 pp., in Technical Report Series on Global Modeling and Data Assimilation, edited by M. J. Suarez, NASA, Greenbelt, MD. (http://ntrs.nasa.gov/archive/nasa/casi.ntrs.nasa.gov/20010072848_2001122986.pdf)

Gurney, K., et al. (2002), Towards robust regional estimates of CO2 sources and sinks using atmospheric transport models, Nature, 415(6872), 626-630, doi:10.1038/415626a.

389 Helfand, H. M., and S. D. Schubert (1995), Climatology of the Simulated Great Plains Low-
390 Level Jet and Its Contribution to the Continental Moisture Budget of the United States, J.
391 Climate, 8(4), 784-806, doi:10.1175/1520-0442(1995)008<0784:COTSGP>2.0.CO;2.
392 Holtslag, A. A. M., and B. A. Boville (1993), Local Versus Nonlocal Boundary-Layer Diffusion
393 in a Global Climate Model, J. Climate, 6(10), 1825-1842, doi:10.1175/1520-
394 0442(1993)006<1825:LVNBLD>2.0.CO;2.
395 Joffre, S. M., M. Kangas, M. Heikinheimo, and S. A. Kitaigorodskii (2001), Variability Of The
396 Stable And Unstable Atmospheric Boundary-Layer Height And Its Scales Over A Boreal
397 Forest, Bound.-Lay. Meteorol., 99(3), 429-450, doi:10.1023/a:1018956525605.
398 Koster, R. D., M. J. Suarez, A. Ducharne, M. Stieglitz, and P. Kumar (2000), A catchment-based
399 approach to modeling land surface processes in a general circulation model: 1. Model
400 structure, J Geophys Res-Atmos, 105(D20), 24809-24822, doi:10.1029/2000jd900327.
401 Lin, S.-J. (2004), A "Vertically Lagrangian" Finite-Volume Dynamical Core for Global Models,
402 Mon. Weather Rev., 132(10), 2293-2307, doi:10.1175/1520-
403 0493(2004)132<2293:AVLFDC>2.0.CO;2.
404 Lock, A. P., A. R. Brown, M. R. Bush, G. M. Martin, and R. N. B. Smith (2000), A New
405 Boundary Layer Mixing Scheme. Part I: Scheme Description and Single-Column Model
406 Tests, Mon. Weather Rev., 128(9), 3187-3199, doi:10.1175/1520-
407 0493(2000)128<3187:anblms>2.0.co;2.
408 Louis, J., M. Tiedtke, and J. Geleyn (1982), A short history of the PBL parameterization at
409 ECMWF, paper presented at Workshop on Planetary Boundary Layer Parameterization,
410 ECMWF, Reading, England.

McMahon, T. A., B. L. Finlayson, A. T. Haines, and R. Srikanthan (1992), Global Runoff - Continental Comparisons of Annual Flows and Peak Discharges, 166 pp., Catena Verlag, Cremlingen, Germany.

Molod, A., and H. Salmun (2002), A global assessment of the mosaic approach to modeling land surface heterogeneity, J Geophys Res-Atmos, 107(D14), 26, doi:10.1029/2001jd000588.

Molod, A., L. Takacs, M. J. Suarez, J. T. Bacmeister, I.-S. Song, and A. Eichmann (2012), The GEOS-5 Atmospheric General Circulation Model: Mean Climate and Development from MERRA to Fortuna 115 pp., in Technical Report Series on Global Modeling and Data Assimilation, edited by M. J. Suarez, NASA, Greenbelt, MD. (http://ntrs.nasa.gov/archive/nasa/casi.ntrs.nasa.gov/20120011790_2012011404.pdf)

Moorthi, S., and M. J. Suarez (1992), Relaxed Arakawa-Schubert. A Parameterization of Moist Convection for General Circulation Models, Mon. Weather Rev., 120(6), 978-1002, doi:10.1175/1520-0493(1992)120<0978:rasapo>2.0.co;2.

Peel, M. C., T. A. McMahon, and B. L. Finlayson (2004), Continental differences in the variability of annual runoff-update and reassessment, J Hydrol, 295(1-4), 185-197, doi:10.1016/j.jhydrol.2004.03.004.

Peel, M. C., B. L. Finlayson, and T. A. McMahon (2007), Updated world map of the Köppen-Geiger climate classification, Hydrol Earth Syst Sc, 11(5), 1633-1644.

Putman, W. M., and S.-J. Lin (2007), Finite-volume transport on various cubed-sphere grids, J. Comput. Phys., 227(1), 55-78, doi: http://dx.doi.org/10.1016/j.jcp.2007.07.022.

Rienecker, M. M., et al. (2008), The GEOS-5 Data Assimilation System—Documentation of Versions 5.0.1, 5.1.0, and 5.2.0 101pp., in Technical Report Series on Global Modeling

433 and Data Assimilation, edited by M. J. Suarez, NASA, Greenbelt, MD.
434 (http://gmao.gsfc.nasa.gov/pubs/docs/GEOS5_104606-Vol27.pdf)
435 Rienecker, M. M., et al. (2011), MERRA: NASA's Modern-Era Retrospective Analysis for
436 Research and Applications, J. Climate, 24(14), 3624-3648, doi:10.1175/jcli-d-11-
437 00015.1.
438 Seibert, P., F. Beyrich, S.-E. Gryning, S. Joffre, A. Rasmussen, and P. Tercier (2000), Review
439 and intercomparison of operational methods for the determination of the mixing height,
440 Atmos. Environ., 34(7), 1001-1027, doi:10.1016/s1352-2310(99)00349-0.
441 Seidel, D. J., C. O. Ao, and K. Li (2010), Estimating climatological planetary boundary layer
442 heights from radiosonde observations: Comparison of methods and uncertainty analysis,
443 J. Geophys. Res., 115(D16), D16113, doi:10.1029/2009jd013680.
444 Seidel, D. J., Y. Zhang, A. Beljaars, J.-C. Golaz, A. R. Jacobson, and B. Medeiros (2012),
445 Climatology of the planetary boundary layer over the continental United States and
446 Europe, J Geophys Res-Atmos, 117(D17106), doi:10.1029/2012jd018143.
447 Stull, R. B. (1988), An introduction to boundary layer meteorology, 666 pp., Kluwer Academic
448 Publishers, Norwell, MA.
449 Triantafyllou, G. N., and A. A. Tsonis (1994), Assessing the ability of the Köppen System to
450 delineate the general world pattern of climates, Geophys Res Lett, 21(25), 2809-2812,
451 doi:10.1029/94gl01992.
452 Vogelezang, D. H. P., and A. A. M. Holtslag (1996), Evaluation and model impacts of
453 alternative boundary-layer height formulations, Bound.-Lay. Meteorol., 81(3-4), 245-269,
454 doi:10.1007/bf02430331.

White, A. B., C. J. Senff, and R. M. Banta (1999), A Comparison of Mixing Depths Observed by Ground-Based Wind Profilers and an Airborne Lidar, J. Atmos. Ocean. Tech., 16(5), 584-590, doi:10.1175/1520-0426(1999)016<0584:acomdo>2.0.co;2.

458

459 Figure 1 Köppen-Geiger climate classes as determined by *Peel et al.* [2007] regridded to the
460 0.5°x0.5° grid used by GEOS-5. The first letter indicates the broad climate class as tropical (A),
461 arid (B), temperate (C), cold (D), and polar (E).

462

463 Figure 2 Scatter plot of PBL depth versus sensible heat flux for the arid, hot desert climate class
464 in winter. Each dot represents the seasonal mean midday PBL depth and sensible heat flux. The
465 PBL depth is defined using the default scalar diffusivity definition in GEOS-5. The Australian
466 deserts are highlighted in color according to evaporative fraction.

467

468 Figure 3 Scatter plot of PBL depth versus 10-meter temperature for the tropical rainforest climate
469 class in the winter. Each dot represents the seasonal mean midday PBL depth and sensible heat
470 flux. The PBL depth is defined using the default scalar diffusivity definition in GEOS-5. The
471 colors highlight the relative humidity.

472

473 Figure 4 Seasonal mean diurnal cycle of PBL depth for climate classes Dsa (Cold with dry, hot
474 summers, during summer and winter, 4a and 4c) and BWh (hot, arid desert, during summer and
475 winter, 4b and 4d) using 7 different methods for estimating the PBL depth.

476

477 Figure 5 Seasonal mean diurnal cycle of PBL depth for climate classes Af (tropical rainforest)
478 during summer (5a) and winter (5b) using 7 different methods for estimating the PBL depth.

479

480 Figure 6 Seasonal mean vertical profile of total and Louis scalar diffusivities (6a) and bulk
481 Richardson number (6b) for JJA in the Amazonian rainforest. The dashed lines represent the
482 PBL depth as determined by method 1 (6a) and method 4 (6b).
483
484 Figure 7 Diurnal cycle of PBL depth response to radiative plumes during JJA. The figure shows
485 the scalar diffusivity method using a 10% of the column maximum threshold including the
486 radiative plume minus the same method, but without the radiative plume. Each subplot is
487 labeled with the current time in UTC.

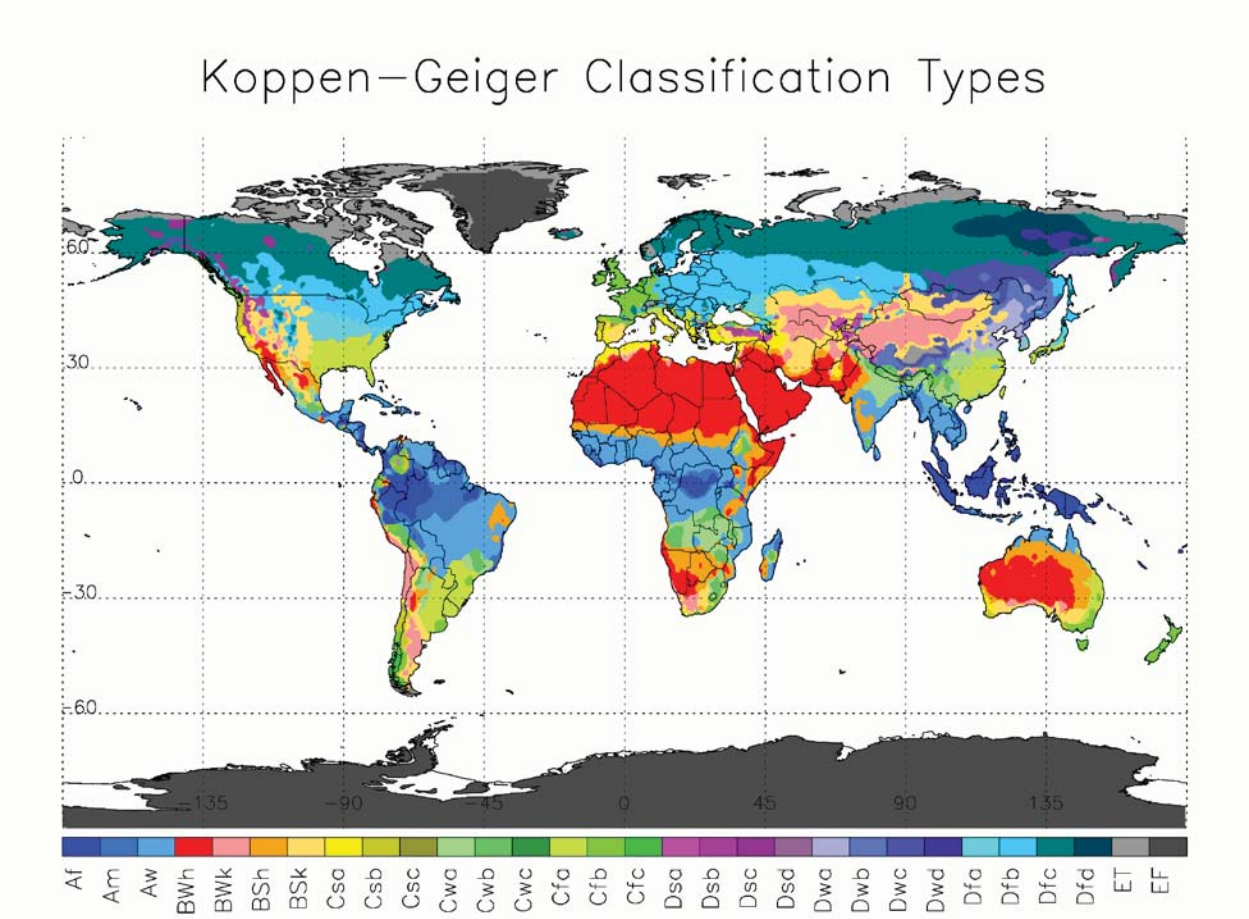

Figure 1 Köppen-Geiger climate classes as determined by *Peel et al.* [2007] regridded to the 0.5°x0.5° grid used by GEOS-5. The first letter indicates the broad climate class as tropical (A), arid (B), temperate (C), cold (D), and polar (E).

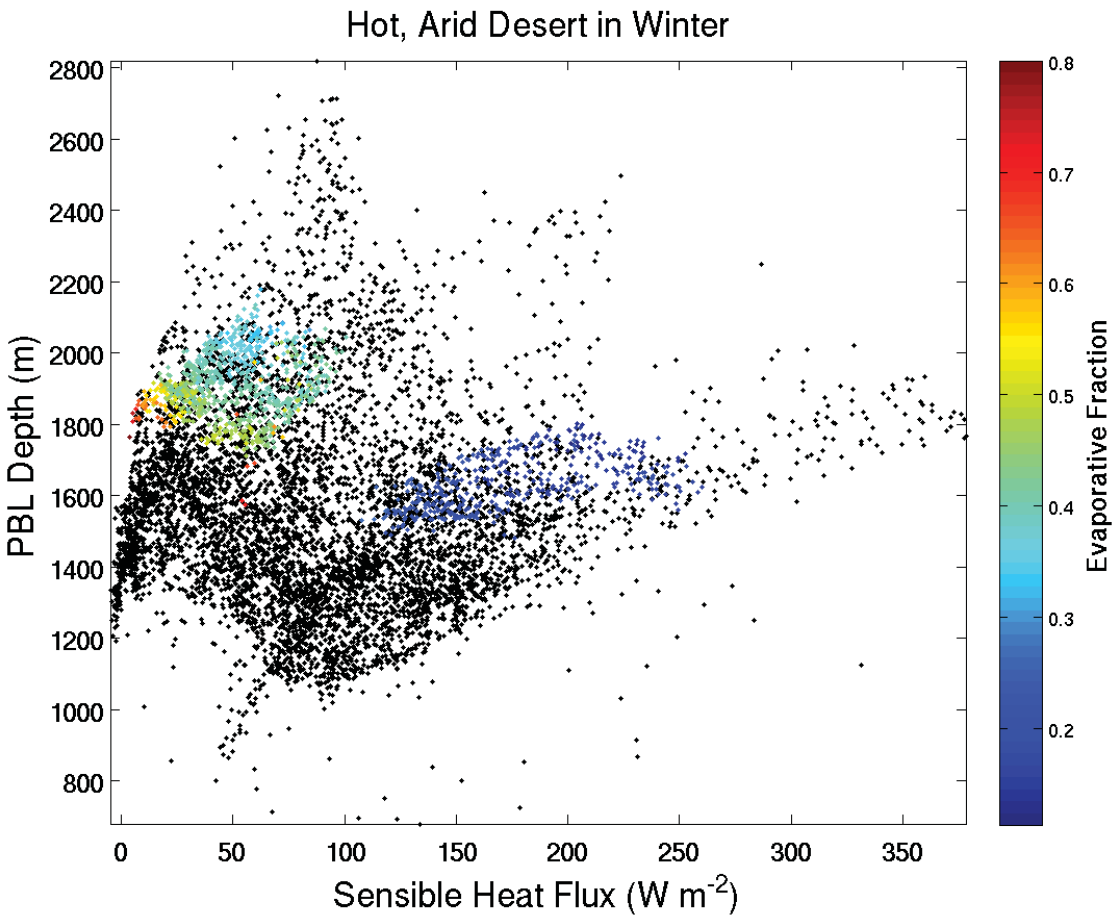

494

495 Figure 2 Scatter plot of PBL depth versus sensible heat flux for the arid, hot desert climate class
496 in winter. Each dot represents the seasonal mean midday PBL depth and sensible heat flux. The
497 PBL depth is defined using the default scalar diffusivity definition in GEOS-5. The Australian
498 deserts are highlighted in color according to evaporative fraction.

499

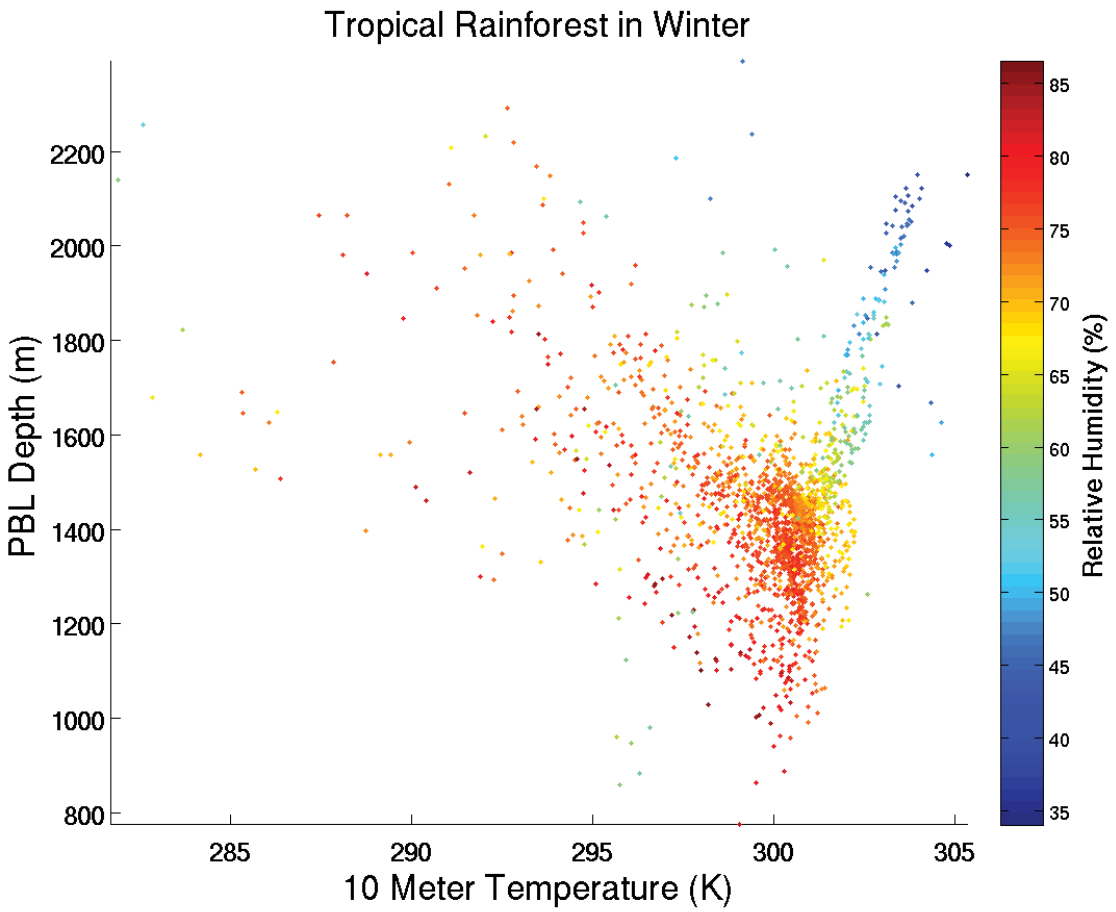

500

501 Figure 3 Scatter plot of PBL depth versus 10-meter temperature for the tropical rainforest climate
502 class in the winter. Each dot represents the seasonal mean midday PBL depth and sensible heat
503 flux. The PBL depth is defined using the default scalar diffusivity definition in GEOS-5. The
504 colors highlight the relative humidity.

505

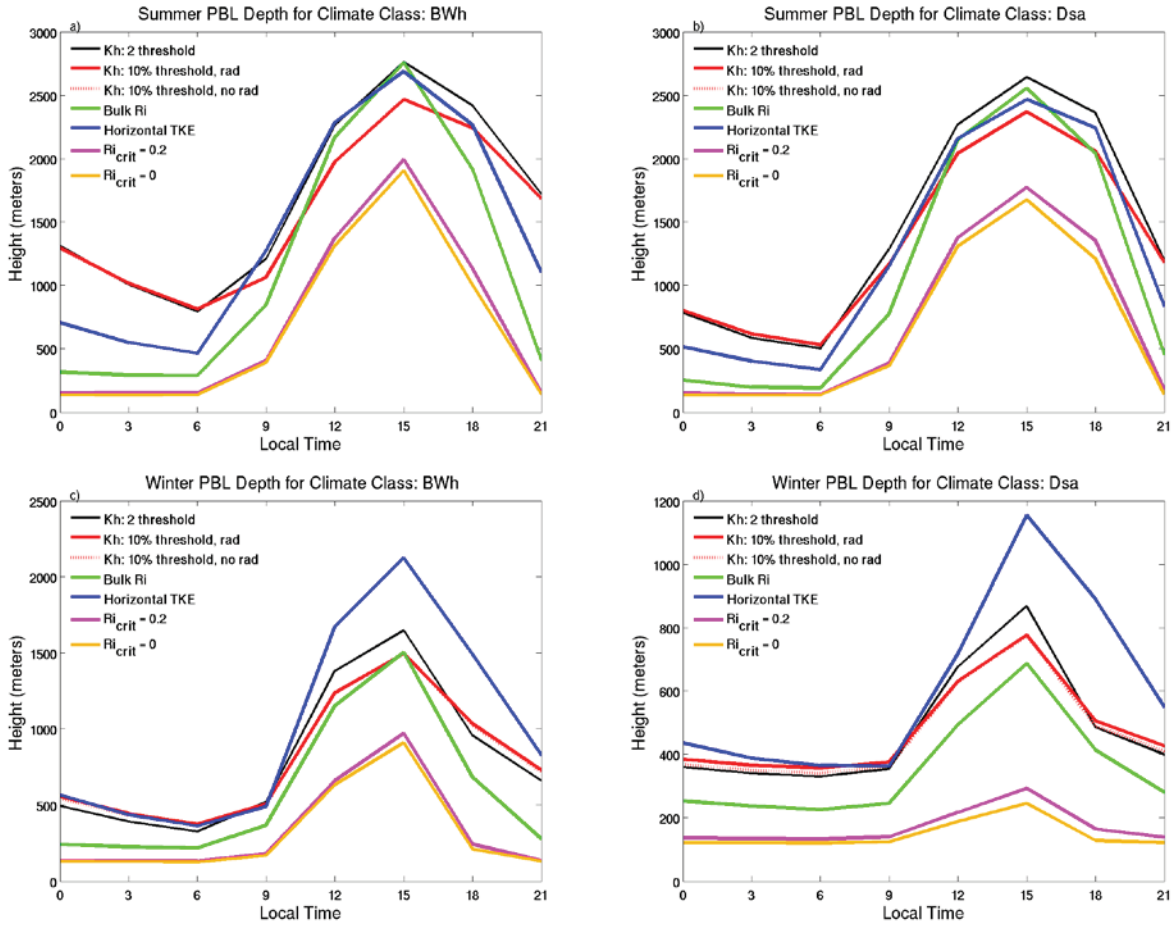

506

507 Figure 4 Seasonal mean diurnal cycle of PBL depth for climate classes Dsa (Cold with dry, hot
508 summers, during summer and winter, 4a and 4c) and BWh (hot, arid desert, during summer and
509 winter, 4b and 4d) using 7 different methods for estimating the PBL depth.

510

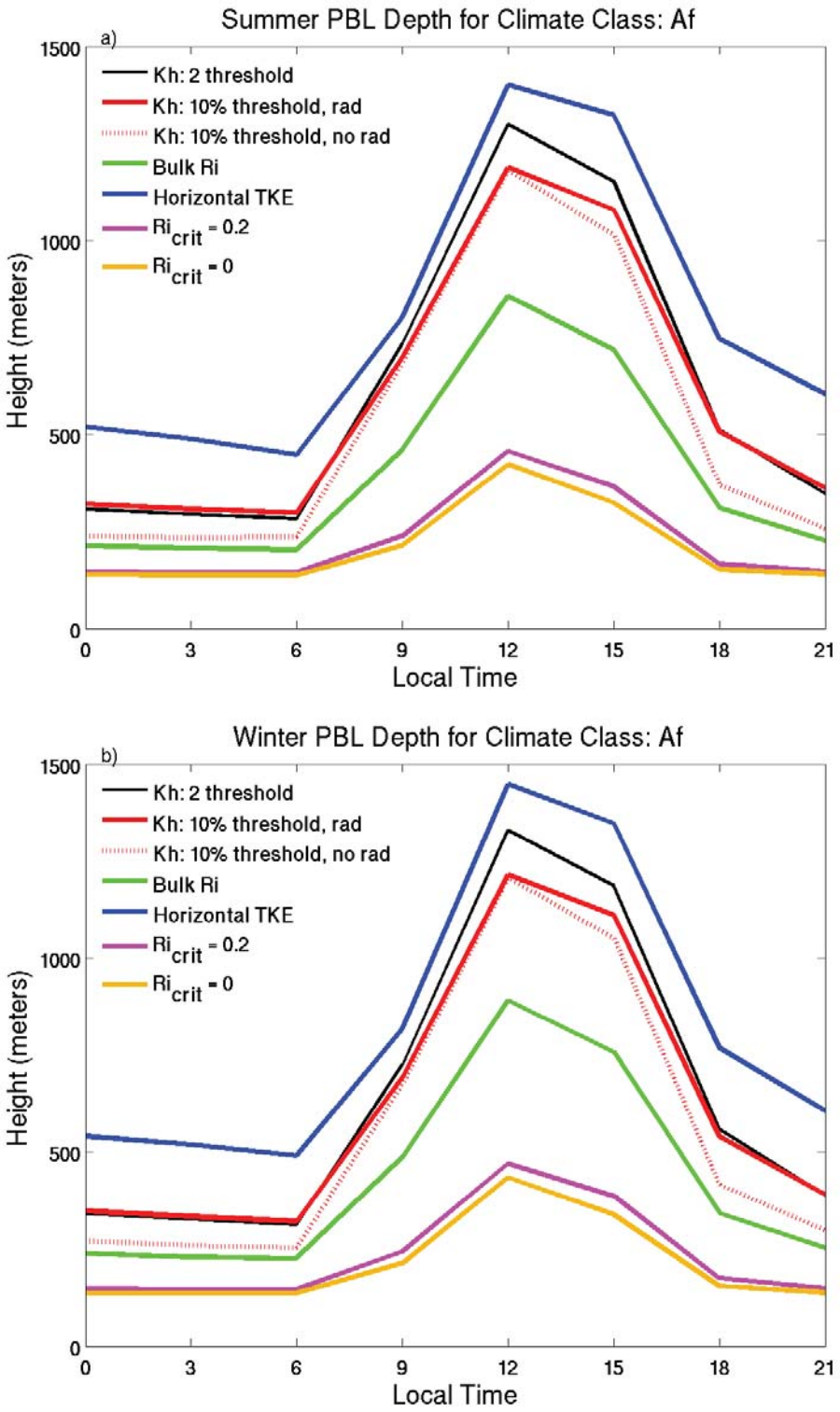

511

512 Figure 5 Seasonal mean diurnal cycle of PBL depth for climate classes Af (tropical rainforest)

513 during summer (5a) and winter (5b) using 7 different methods for estimating the PBL depth.

514

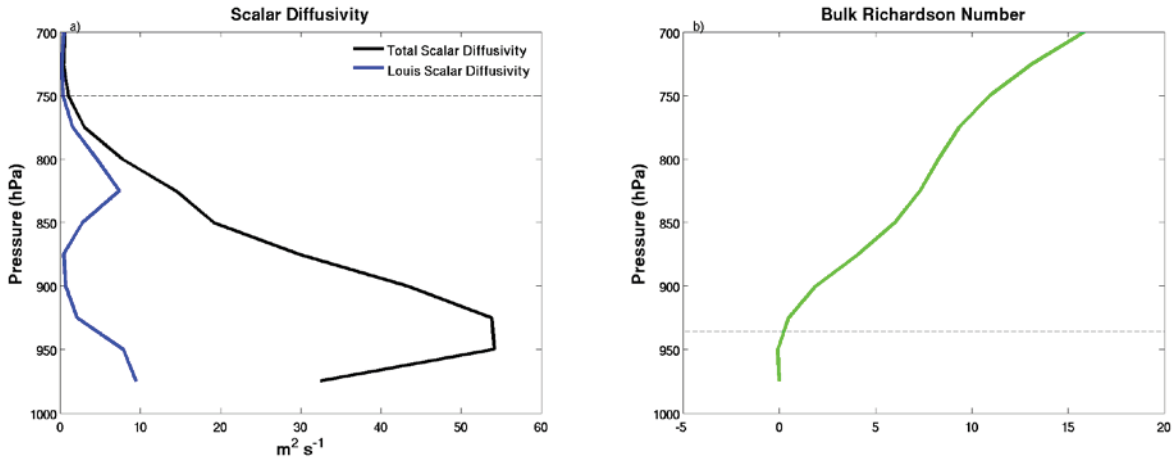

515

516 Figure 6 Seasonal mean vertical profile of total and Louis scalar diffusivities (6a) and bulk
517 Richardson number (6b) for JJA in the Amazonian rainforest. The dashed lines represent the
518 PBL depth as determined by method 1 (6a) and method 4 (6b).

519

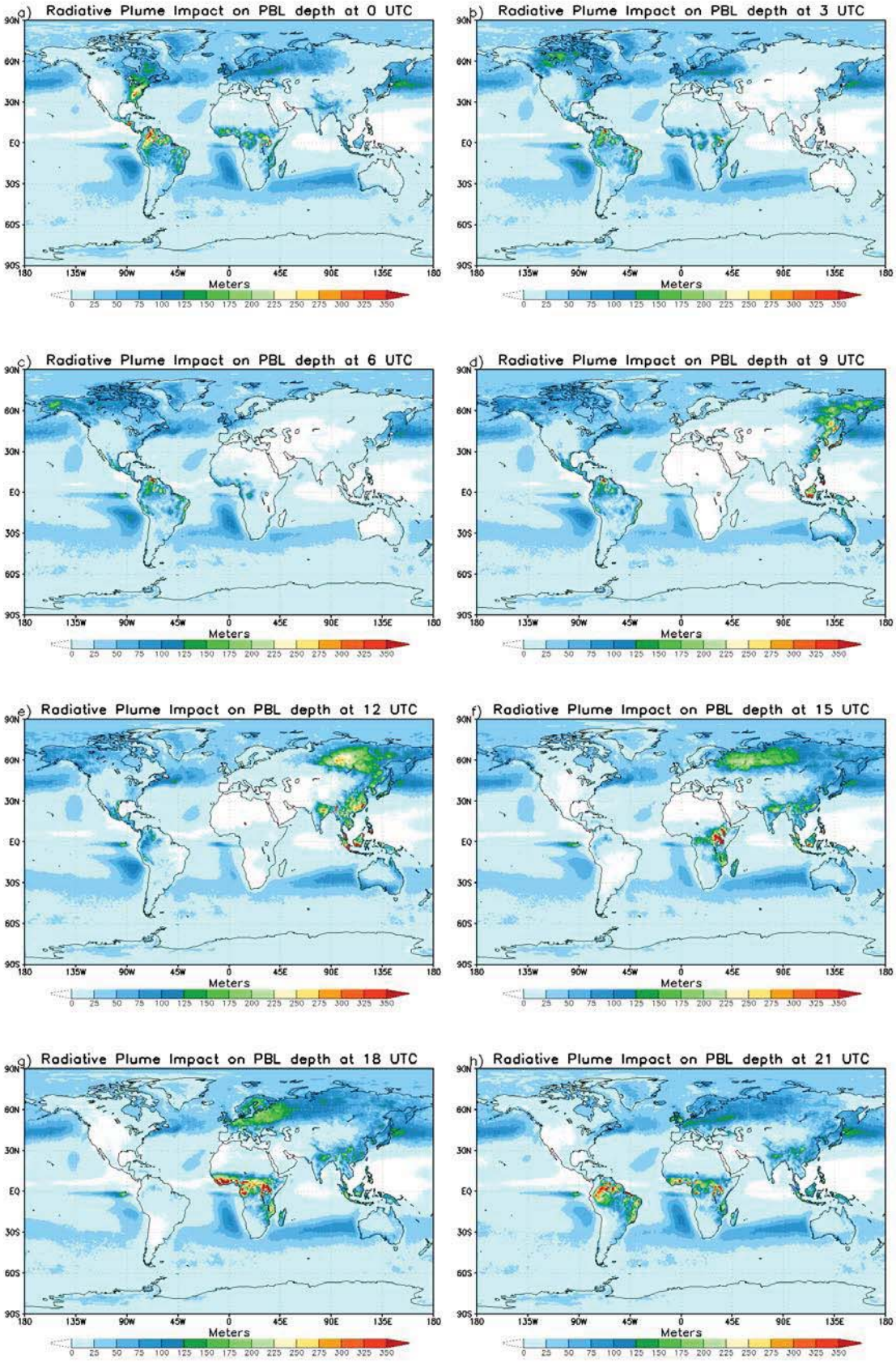
a) Radiative Plume Impact on PBL depth at 0 UTC
b) Radiative Plume Impact on PBL depth at 3 UTC
c) Radiative Plume Impact on PBL depth at 6 UTC
d) Radiative Plume Impact on PBL depth at 9 UTC
e) Radiative Plume Impact on PBL depth at 12 UTC
f) Radiative Plume Impact on PBL depth at 15 UTC
g) Radiative Plume Impact on PBL depth at 18 UTC
h) Radiative Plume Impact on PBL depth at 21 UTC
90N
60N
30N
EQ
30S
60S
90S
180
135W
90W
45W
0
45E
90E
135E
180
Meters
0 25 50 75 100 125 150 175 200 225 250 275 300 325 350

520

Figure 7 Diurnal cycle of PBL depth response to radiative plumes during JJA. The figure shows the scalar diffusivity method using a 10% of the column maximum threshold including the radiative plume minus the same method, but without the radiative plume. Each subplot is labeled with the current time in UTC.

525

526

527 Summary of PBL depth Methods

Method	Abbreviation	Description
1	Kh: 2 threshold	Uses total scalar diffusivity and a threshold of 2 $m^2 s^{-1}$, this is the default PBL depth in GEOS-5
2	Kh: 10% threshold, rad	Uses total scalar diffusivity and a threshold equal to 10% of the column maximum, includes the radiative plume
3	Kh: 10% threshold, no rad	Uses total scalar diffusivity and a threshold equal to 10% of the column maximum, does not include the radiative plume
4	Bulk Ri	Uses the bulk Richardson number used by *Seidel et al.* [2012] and a critical value of 0.25
5	$Ri_{crit} = 0.2$	Uses a Richardson number and a critical value of 0.2
6	$Ri_{crit} = 0$	Uses a Richardson number and a critical value of 0
7	Horizontal TKE	Uses the diagnosed horizontal turbulent kinetic energy and a threshold of 10% of the column maximum

528

529 Table 1 List of the PBL depth methods used along with the abbreviations.